Benchmarking Charge-Transfer Excited States in TADF Emitters: ΔDFT outperforms TD-DFT for Emission Energies

Thomas Froitzheim,[1,*] Lukas Kunze,[1,*] Stefan Grimme,[1] John M. Herbert,[2] and Jan-Michael Mewes[1,†]

[1] *Mulliken Center for Theoretical Chemistry, University of Bonn, Beringstr. 4, 53115 Bonn, Germany*
[2] *Department of Chemistry and Biochemistry, The Ohio State University, Columbus, Ohio 43210, United States*

(Dated: May 17, 2024)

Charge-transfer excited states are crucial to modern electronics, particularly organic light-emitting diodes (OLEDs) based on thermally-activated delayed fluorescence (TADF). However, accurately modeling CT states remains challenging, even with modern implementations of (time-dependent) density functional theory [(TD-)DFT], especially in a dielectric environment. To identify shortcomings and improve the methodology, we previously established the STGABS27 benchmark set with highly accurate experimental references for the adiabatic energy gap between the lowest singlet and triplet excited states (ΔE_{ST}).[1] Here, we diversify this set to the STGABS27-EMS benchmark by including experimental emission energies (E_{em}) and use this new set to (re)-evaluate various DFT-based approaches. Surprisingly, these tests demonstrate that a state-specific (un)restricted open-shell Kohn-Sham (U/ROKS) DFT coupled with a polarizable continuum model for perturbative state-specific non-equilibrium solvation (ptSS-PCM) provides exceptional accuracy for predicting E_{em} over a wide range of density functionals. In contrast, the main workhorse of the field, Tamm-Dancoff-approximated TD-DFT (TDA-DFT) paired with the same ptSS-PCM, is distinctly less accurate and strongly functional dependent. More importantly, while TDA-DFT requires the choice of two very different density functionals for good performance on either ΔE_{ST} or E_{em}, the time-independent U/ROKS/PCM approaches deliver excellent accuracy for both quantities with a wide variety of functionals.

Keywords: Thermally-activated delayed fluorescence, Charge-transfer excited states, Excited-state solvation

I. INTRODUCTION

The rise of computation-driven rational design in organic electronics and materials necessitates the robust and accurate prediction of optoelectronic properties. [2–8] Next-generation organic light-emitting diodes (OLEDs) based on thermally activated delayed fluorescence (TADF) are a prominent example. TADF emitters harvest both singlet and triplet excitons through the transfer of excitons via (reverse) intersystem crossing [(r)ISC]. Since the rate of population transfer depends exponentially on the adiabatic energy gap ΔE_{ST} between the lowest singlet (S_1) and triplet (T_1) excited states, it imposes a tight constraint on TADF emitter design. One way to achieve small singlet-triplet gaps on the order of the thermal energy ($k_{\mathrm{B}}T \approx 0.025\,\mathrm{eV}$) is by spatially separating electron and hole in charge-transfer (CT) excited states. Accordingly, the computational study of CT states and the accurate prediction of their relative energies have attracted great interest.

To assess the accuracy of commonly applied methods for the CT state of TADF emitters, some of us previously introduced the STGABS27 benchmark set,[1] consisting of 27 emitters with highly accurate experimental ΔE_{ST} values obtained from temperature-dependent measurements of the TADF rate.[9] Our work demonstrated that state-specific restricted or unrestricted open-shell Kohn-Sham density functional theory (ROKS or UKS)[10–13] combined with a polarizable continuum solvation model (PCM)[14, 15] yields ΔE_{ST} with a remarkably small error of $\approx 0.5\,\mathrm{kcal/mol}$, which we attributed to the full inclusion of orbital relaxation and dielectric screening in the method. Notably, this result within chemical accuracy remains remarkably stable across various density functionals from the classical PBE0-D4 (mean absolute error, MAE: 0.029 eV) to the state-of-the-art optimally tuned (OT) range-separated hybrid (RSH) functional OT-ωB97M-V (MAE: 0.021 eV). In stark contrast, some of us showed in a recent paper[16] that the accuracy of time-dependent density functional theory in the Tamm-Dancoff approximation (TD(A)-DFT[17–19]) depends strongly on the chosen functional and solvation model. For most method combinations, outliers dominate the results, leading to deviations frequently exceeding the absolute ΔE_{ST} values. Only functionals with a small fraction of Fock exchange ($\approx$10%) applied in vertical approximation (i.e., using ground-state structures) and evaluated without a proper solvent model approach the accuracy of ΔDFT/PCM (MAE: 0.042 eV), which we attributed to strong error-cancellation effects. Accordingly, the good performance of this approach comes at the expense of overly stabilized CT states, sometimes by up to 1 eV, reminiscent of the CT failure of pure (meta-)GGA functionals.[20, 21] To better identify such unreliable error-compensation-based methods and improve the diversity of the STGABS27 benchmark, we decided to include experimental emission energies E_{em}, which probe the energy difference between the polar excited CT (S_1) and the non-polar ground state (GS). As such, emission energies offer a complementary challenge to the energy

* These two authors contributed equally.
† Corresponding author: janmewes@janmewes.de

difference between two similar CT states (S_1 and T_1) in the original set, in which error-cancellation effects are much less helpful.

Countless previous studies have explored theoretical methods for calculating transition energies from and to CT excited states. For the sake of conciseness, we limit the following discussion to the most relevant ones. Shee and Head-Gordon recently investigated TD-DFT with a perturbative (pt)SS-PCM solvation model for the absorption and emission energies of twist-induced (TI)CT excited states, including some TADF emitters.[22] They found optimally tuned RSH functionals such as OT-LC-ωPBE perform particularly well. Nonetheless, limitations of single-excitation-based TD-DFT persist, especially for smaller systems, which they attribute to missing orbital relaxation. Although they demonstrated that state-specific ΔROKS mitigates these errors, their approach lacked a proper account for solvation (they were taken from the TD-DFT calculations). A series of benchmarks by Jacquemin *et al.* on realistically-sized organic emitters underscores the advantages of (OT-)RSH functionals.[23–27] Moreover, they emphasize the critical role of a state-specific non-equilibrium solvation model for treating CT states accurately. In another work, Jacquemin *et al.* explored the influence of correlation within a set of theoretical reference data for 30 intramolecular CT transitions.[28] Unfortunately, the prohibitive computational cost of high-level calculations limited the system size to only the smallest CT systems, in which orbital relaxation and dielectric stabilization are less important. While an RSH functional (ωB97X-D[29]) is again the most accurate with pure TD-DFT, more sophisticated wavefunction-based methods such as second-order algebraic diagrammatic construction ADC(2)[30, 31] or second-order approximate coupled cluster CC2[32] provide some improvements. These findings were recently corroborated by Mester and Kállay,[33] further suggesting a benefit from an accurate explicit description of orbital relaxation. In this work, we want to systematically expand the benchmarking of CT emission energies in solution to ΔDFT-based methods including a complete non-equilibrium solvation model. To this end, we implemented non-equilibrium state-specific solvation for ΔDFT in the Q-Chem program.[34]

This work adheres to the following structure: In section II, we present the reference values for the expansion of the STGABS27 set. Sections III and IV outline the theory and technical details necessary for calculating vertical emission energies with TDA-DFT and ΔDFT. Lastly, in section V, we illustrate the specific emission energies and the statistical performance of various density functionals on the expanded STGABS27 set to derive general recommendations for treating solvated CT states.

TABLE I. Names, measurement conditions, experimental E_{em} value (in eV), and literature references for all emitters of the STGABS27-EMS set.

No.	name	solvent[a]	E_{em}[h]	ref.
1	MCz-XT	5 wt %:PPF[b]	2.59	[35]
2	TMCz-BO	10 μmol, tol.[c]	2.78	[36]
3	FAc-XT	5 wt %:PPF	2.54	[35]
4	PTZ-DBTO2	dilute tol.	2.12	[37]
5	ACRXTN	5 mol %:mCP[d]	2.59	[38]
6	PHOX-$^{\mathrm{Me}}\pi$	20 μmol, tol.	1.99	[39]
7	PXZ-$\mathrm{Mes_3B}$	10 μmol, tol.	2.44	[40]
8	TPA-PH2CN	10 μmol, tol.	2.52	[41]
9	oTE-DRZ	10 μmol, tol.	2.35	[42]
10	DACT-II	6 wt %:CBP[e]	2.40	[43]
11	XAc-XT	5 wt %:PPF	2.58	[35]
12	5Cz-TRZ	dilute tol.	2.48	[44]
13	2DAC-$\mathrm{MES_3B}$	10 μmol, tol.	2.51	[40]
14	MFAc-OPS	10 μmol, tol.	2.80	[45]
15	MFAc-SPS	10 μmol, tol.	2.73	[45]
16	p-AC-DBNA	10 μmol, DCM[f]	2.23	[46]
17	3ACR-TRZ	10 μmol, tol.	2.43	[47]
18	m'-AC-DBNA	10 μmol, DCM	2.18	[46]
19	TPA-cNDI	10 μmol, tol.	1.65	[48]
20	4CzIPN	10 μmol, tol.	2.45	[49]
21	3DPA3CN	tol.	2.45	[50]
22	5CzBN	10 μmol, tol.	2.64	[49]
23	p-2Cz2BMe	10 μmol, tol.	2.22	[51]
24	ACRFLCN	6 wt %:TPSi-F[g]	2.56	[52]
25	Spiro-CN	6 wt %:mCP	2.30	[53]
26	DABNA-2	20 μmol, DCM	2.64	[54]
27	DABNA-1	20 μmol, DCM	2.68	[55]

a) If no value for n^2 is known 2.25 (toluene)[56] is used.
b) 2,8-bis(diphenylphosphoryl)dibenzo[b,d]furan: $\varepsilon = 5.0$[57].
c) Toluene: $\varepsilon = 2.37$, $n^2 = 2.25$.
d) N,N'-dicarbazolyl-3,5-benzene: $\varepsilon = 2.84$.[58]
e) 4,4'-bis(carbazol-9-yl)biphenyl: $\varepsilon = 3.5$ (see SI)
f) Dicholoromethane: $\varepsilon = 8.93$, $n^2 = 2.03$.[56]
g) Triphenyl-(4-(9-phenyl-9H-fluoren-9-yl)phenyl)silane: $\varepsilon = 2.5$.[59]
h) Estimated accuracy $\pm$0.02-0.06 eV in the given spectral region.

II. BENCHMARK SET

To thoroughly judge the applicability of an excited state method for the CT states of TADF emitters, we extended the STGABS27 benchmark set with experimental emission energies E_{em} for all included systems. This new benchmark set shall be named STGABS27-EMS. Table I summarizes the key data, including reference emission energies, experimental measurement conditions, and corresponding literature references.

In contrast to the singlet-triplet gaps in STGABS27 where careful consideration of the experimental method was crucial to ensure reliable data for the mostly tiny energy differences < 0.1 eV, the 10-20 times larger emission energies can be taken from standard fluorescence spectra reported in the original publications. We primarily rely on the peak maximum or photoluminescence wavelength λ_{PL}. Where λ_{PL} was not explicitly stated

(molecules 4, 12, 20, 22, and 25), we extracted the maximum position from the reported fluorescence spectra. Since polar CT states present in all but the MR-TADF emitters DABNA-1 (27) and DABNA-2 (26) exhibit a large bandwidth for the fluorescence peaks, we assume a statistical uncertainty in the emission energy of up to 10 nm ($0.02 - 0.06$ eV in the spectral region between $440 - 750$ nm).

Further, we want to acknowledge that the fluorescence maximum typically does not directly correspond to the vertical emission energy at the optimized excited state geometry. Discrepancies arise from differences in zero-point vibrational energy (ZPVE) between ground and excited state or vibrational effects leading to deviations from strictly vertical transitions.[23, 60] Unfortunately, the strong S_1 CT character prevents a more well-founded comparison to 0-0 transitions, as the required absorption peak is typically weak and broad.[61] Moreover, 0-0 transitions, i.e., equilibrium-to-equilibrium, are not suitable for testing non-equilibrium solvation corrections for state-specific ΔDFT, which is a side goal of this work. Thus, we will compare E_{em} to the fluorescence maximum, arguing that this still provides valuable insights since most donor-acceptor type TADF emitters are rather similar regarding their electronic and chemical structure, which should lead to rather systematic deviations. Facing the same issue, other authors assume an uncertainty of absolute vertical emission energies ranging between 0.1 and 0.2 eV, of which we chose the latter as a conservative estimate.[22, 23, 60, 62, 63].

III. THEORY: SOLVATION FOR VERTICAL TRANSITIONS

In the following, we briefly introduce the theoretical background for calculating vertical transition energies in the presence of a dielectric continuum. We omit a comprehensive review of the underlying theory for polarizable continuum models (PCM) and instead refer the reader to relevant literature.[15, 64–70] Throughout, we follow the notation established in ref. 15, where a reaction field operator $\hat{R}_i$ of state $|\Psi_i\rangle$ polarizes the continuum and leads to the following state-specific Schrödinger equation

$$\left(\hat{H}^{\mathrm{vac}} + \hat{R}_i\right)|\Psi_i\rangle = E_i|\Psi_i\rangle. \tag{1}$$

Since electronic transitions occur on a much shorter timescale than the structural relaxation of the solute, the polarization response to the transition can be split into two parts, which can be regarded as the application of the Frank-Condon principle to the solvent: On the one hand, there is a fast electronic response from the solvent electronic degrees of freedom (DOF) that can follow the changing charge distribution of the solute, and on the other a slow orientational and vibrational response of the solvent nuclear DOFs, which remain unchanged. Therefore, we need to partition the total reaction field

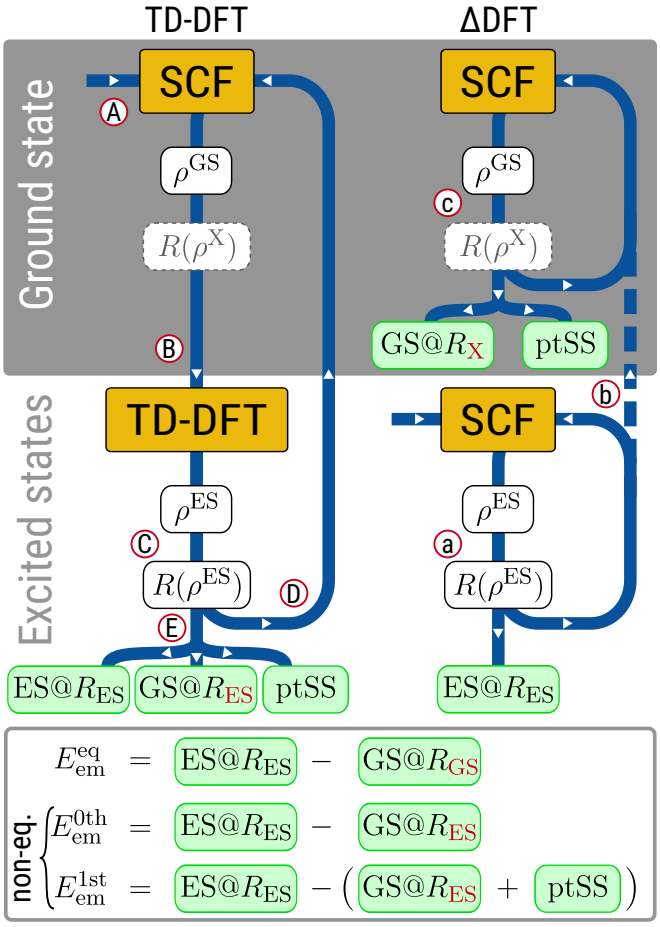

FIG. 1. Schematic overview for the calculation of emission energies with either TD-DFT (left) or ΔDFT (right) in solution. White boxes indicate intermediates (the dashed $R(\rho^x)$ is replaced after the first iteration by the frozen excited state reaction field of the excited state), while green boxes indicate final results. Letters A-E in the TD-DFT and letters a-c in the ΔDFT procedure mark sections referenced in the text.

($\propto \varepsilon$) into a fast part ($\propto \varepsilon_\infty = n^2$, with the refractive index n), and a remaining slow part [71–75]

$$\hat{R} = \hat{R}^f + \hat{R}^s. \tag{2}$$

Accordingly, during a vertical transition from the equilibrium initial state fulfilling equation 1 (e.g., some excited state for emission) to the non-equilibrium final state, only the fast component $\hat{R}^f$ relaxes. Consequently, the Hamiltonian of the final state depends on both the fast component of its own and the slow component of the initial reaction field

$$\hat{H}_{\mathrm{final}} = \hat{H}^{\mathrm{vac}} + \hat{R}^f_{\mathrm{final}} + \hat{R}^s_{\mathrm{initial}}. \tag{3}$$

The energy difference between the initial and final states defines the vertical emission energy E_{em}.

However, the strict application of this scheme results in a computationally demanding iterative approach and non-orthogonal states. To sidestep such complications,

we avoid the interdependence between the initial and final states in the Hamiltonian by approximating the relaxation of $\hat{R}^f$ for the final state by perturbation theory (denoted ptSS-PCM[68], closely related to the corrected linear-response (cLR)-PCM[76]), using the usual perturbation expression

$$\hat{R}^f_{\text{final}} = \hat{R}^f_{\text{initial}} + \lambda \left(\hat{R}^f_{\text{final}} - \hat{R}^f_{\text{initial}} \right). \tag{4}$$

The clear advantage of the perturbative approach is that the 1st-order perturbative approximation of the fast response of the final state ($E^{\text{1st}}_{\text{em}}$, compare Figure 1), can be obtained in a single step once the excited-state density is known.

Excitation- and ΔSCF-based procedures — Below, we detail the calculation of the initial excited and the final ground state with excitation- and ΔSCF-based methods, now integrated into the latest version of the Q-Chem program.[34]

In the state-specific (SS-)PCM formalism for excitation-based methods [65, 66, 69, 76–83], such as configuration interaction (CI[84]), algebraic diagrammatic construction (ADC(n)[30, 31]), equation-of-motion/linear-response coupled cluster (EOM/LR-CC[85, 86]), or most relevant here TD(A)-DFT, the reaction field enters the calculation through the "solvated" ground state orbitals. Consequently, to equilibrate the initial excited state, its reaction field has to be coupled back into the ground state SCF. This is done in a procedure known as PerTurbation of Energy and Density (PTED) SS-PCM, illustrated on the left of Figure 1.[69] It begins with a ground state SCF calculation, usually including a PCM (A) to produce initial orbitals for the excited state TD-DFT calculation (B). From the TD-DFT calculation, we obtain the excited state density used subsequently to polarize the continuum and yield the excited state reaction field (C). This reaction field enters unchanged (frozen reaction field) into the next ground state SCF (D), which produces an updated set of orbitals to return to step (B). Hence, at the high computational cost of repeated (iterative) calculation of the excited states, the PTED approach prepares both ground and excited states in the reaction field of the targeted excited state. Combined with the perturbative non-equilibrium approach described above (E), this allows the direct calculation of vertical emission energies.

For ΔSCF-based methods, the procedure depicted on the right of Figure 1 is more straightforward than for excitation-based methods, which originates in the state-specific nature of the ΔSCF approach: The inherent separation of the ground and excited state calculations in two distinct SCFs enables the concurrent optimization of the excited state reaction field and the excited state density (a), i.e., without the need to repeat the entire ground and excited state computation until convergence. Since isolated calculations yield each state under equilibrium conditions, the converged reaction field of the initial excited state must enter the final ground state (b). Ultimately, only a single SCF in this frozen reaction field is necessary (c) for the final ground state and the ptSS-PCM correction.

Let us finish with a few words about the nomenclature used in the following:

- ptSS-PCM always refers to the first-order corrected non-equilibrium transition energy. In the case of absorption, this means the ground state equilibrated PCM and a ptSS-PCM term for relaxation to the excited state, and, in the case of emission (relevant here), it means the excited state equilibrated PCM and a ptSS-PCM term for relaxation to the ground state ($E^{\text{1st}}_{\text{em}}$ in Figure 1).

- SS-PCM refers to fully equilibrated state energies, i.e., the lack of any ptSS non-equilibrium corrections ($E^{\text{eq}}_{\text{em}}$). For this, excitation-based methods require an iterative solvent-field optimization for each state (left of Figure 1), whereas full equilibration is the "natural" result in state-specific ΔDFT approaches. This would be the physically correct model for modeling 0-0 transitions.

- Just "PCM" refers to calculations using the ground state reaction field, i.e., no excited states are considered for solvation (correct for absorption at 0th-order, $E^{\text{0th}}_{\text{abs}}$). This is the "natural" result of excitation-based approaches (when using solvated orbitals), while it does not naturally occur in ΔDFT approaches. Even though such ground state solvation is incorrect for emission calculations (TDA-DFT calculation for the excited state structure), it is the default in some QC programs.

- Finally, the linear-response (LR-)PCM[87] is the default solvation model for TD-DFT in many QC programs also for excited state optimizations, since analytical gradients are available. However, as known for a long time, LR-PCM fails to recover the strong polarization response of CT states (see below).[68, 88–90]

- Correct conditions for an emission calculation with the reaction field fixed to the excited state ($E^{\text{0th}}_{\text{em}}$) require an SS-PCM calculation only for the initial state, termed $\text{SS}^{\text{initial}}$-PCM. While excitation-based methods with SS-PCM yield naturally the final ground state in the reaction field of the initial excited state, ΔDFT requires a specific frozen reaction field SCF.

IV. COMPUTATIONAL DETAILS

All calculations were performed with a development version of the Q-Chem 5.4.2 program, containing the solvation model developments for TD(A)-DFT and ΔDFT described in section III. Emission energies were generally

calculated in the vertical approximation at the relaxed structure of the first excited singlet state S_1, optimized at the same level of the theory. Since the state-specific PCM formalism for TDA-DFT lacks analytical nuclear gradients, geometry optimizations were carried out with TDA-DFT in the gas phase. Aside from exploratory calculations, all emission energies were calculated with state-specific PCM solvation with non-equilibrium effects added perturbatively via the ptSS-PCM (vide supra). The reaction field was divided into fast and slow components according to the Marcus partition,[91, 92] with the required parameters ε and n for each solvent taken from the Minnesota Solvent Descriptor Database.[56]

Our selection of density functional approximations (DFAs) covers a range of global and optimally tuned[93, 94] range-separated hybrid functionals mostly based on PBE[95]. For the global hybrids, the fraction a_x of admixed exact exchange varies between 10% for PBE10, 25% for PBE0,[96] and 37.5% for PBE38.[97] By interpreting a_x as a screening of electron-hole attraction in TDA-DFT calculations ($a_x = \frac{1}{\varepsilon}$), these admixtures equate to dielectric screening factors between $\varepsilon = 10$ (10%) and 2.6 (37.5%). For the range-separated hybrid functionals, we selected the optimally tuned LC-ωPBE (OT-LC-ωPBE, 0-100%)[98] and LRC-ωPBEh (OT-LRC-ωPBEh, 20-100%)[99] as well as the best performer for singlet-triplet gaps on the STGABS27 set, the optimally tuned ωB97M-V (OT-ωB97M-V, 15-100%)[100] functional. We omit untuned RSH functionals, as extensive prior studies found that the standard ω values, typically optimized for ground state thermochemistry, are too large for excited state applications.[1, 22, 25] The optimally tuned range-separation parameters ω were taken from ref. [1]. All calculations employ the DFT-D4 dispersion correction,[101, 102] using for OT-RSHs the same damping parameters as in the untuned functional.[103] Furthermore, all calculations employ the def2-SVP basis set[104, 105] (see the Supporting Information for a detailed basis set study).

V. RESULTS AND DISCUSSION

The example of MCz-XT — Let us begin with an in-depth comparison of solvation effects at either the TDA-DFT or ΔDFT level, using 1,3,6,8-tetramethylcarbazole-xanthone (MCz-XT, molecule 1) as an example. Figure 2 shows the energy shifts caused by the dielectric environment for the ground (GS, blue), as well as the lowest CT (green) and LE (red) excited states of MCz-XT. Starting with MCz-XT in vacuum at the ground state geometry (middle), both TDA-DFT and ΔUKS predict the CT and LE at around 3.7 eV, but with different ordering. TDA-DFT favors the CT state, while ΔUKS predicts a near degeneracy. For D-A TADF emitters containing extended π-systems, such as MCz-XT, near degeneracies between low-lying CT and LE states are common. Upon structural relaxation, either the CT or LE state can become the lowest one.

If we now include the dielectric environment, three distinct scenarios have to be considered, depending on the choice of the state for geometry optimization: (i) vertical absorption at the relaxed ground state structure, as well as vertical emission at either (ii) the CT or (iii) LE excited state structure. Let us begin with the optimized ground state structure (i). Under equilibrium solvation conditions for each state (SS-PCM, solid levels), we find a consistent stabilization for all states w.r.t. the vacuum. The effect is more pronounced for the polar CT state (-0.69 or -0.86 eV) than in the less polar GS and LE state (-0.26 to -0.35 eV). Consequently, the CT state is invariably the lowest excited state. However, this is not as unambiguous under non-equilibrium conditions appropriate for modeling vertical absorption. Without any relaxation of the final excited state reaction field (0th-order neq., $\mathrm{SS}^{\mathrm{initial}}$, dashed levels), the relative excited state levels remain almost unchanged compared to the vacuum. In particular, the CT state experiences no special stabilization since the non-polar GS only weakly polarizes the dielectric environment. Only the relaxation of the fast solvent DOFs to the specific excited state via the ptSS-PCM (1st-order neq., dotted levels) drives the CT below the LE states and yields lower CT absorption energies ($E_{\mathrm{abs}}^{\mathrm{1st,CT}} < E_{\mathrm{abs}}^{\mathrm{1st,LE}}$). While the CT remains equal for TDA-DFT and ΔDFT, the absorption energies to the LE still reflect the initial gas phase energy discrepancy.

Moving on to the excited state structures of CT (ii) and LE (iii), we identify two main factors for the vertical emission energies of either state at its optimal geometry, namely, (a) the overall stabilization due to the dielectric environment, and (b) the non-equilibrium effect on the ground state. For factor (a), we begin again with equilibrium solvation conditions. Compared to the ground state structure, both states experience an additional energy lowering after state-specific geometry optimization. This seems to be dominated by the geometric relaxation of the solute as both CT and LE states respond similarly ($\approx$0.25-0.3 eV, with either TDA-DFT or ΔUKS).

As for vertical absorption, non-equilibrium solvation (b) plays a crucial role for E_{em}. Whereas non-equilibrium solvation effects increase vertical absorption energies, vertical emission energies are consistently decreased compared to treating all states in their respective equilibrium conditions. The polarized CT reaction field greatly destabilizes the non-polar ground state (+0.4-0.6 eV for 0th-order and +0.2-0.3 eV 1st-order solvation) while non-equilibrium effects for emission from the LE state are negligible (below 0.1 eV). This destabilization is mostly due to the polarization work, which amounts to half of the interaction energy of the initial state (here CT) with its self-induced polarization. Because the polar CT strongly polarizes the environment, the polarization work is large whereas the interaction with the non-polar ground state is small. Together, this results in a pronounced destabilization of the GS.[69]

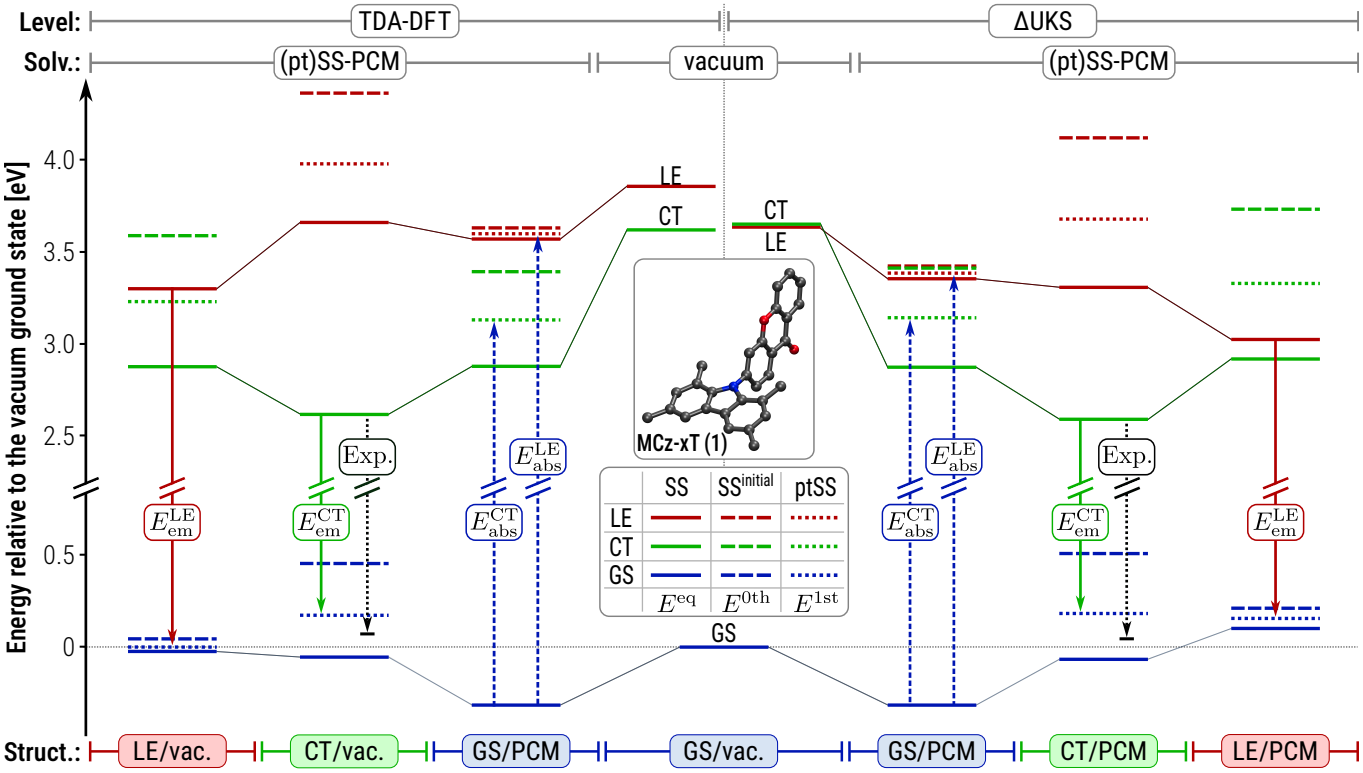

FIG. 2. Energy level diagram for the TDA-DFT (left) and ΔUKS (right) calculation of absorption (dashed arrows) and emission energies (solid arrows) for the lowest charge-transfer (CT, green) and locally excited (LE, red) states of MCz-XT (molecule 1) in PPF matrix ($\varepsilon = 5.00$, $n^2 = 2.25$) solvation. All calculations employ the OT-ωB97M-V functional. For each possible initial state [ground state (GS, blue), CT, and LE], geometries indicated at the bottom are optimized (for TDA-DFT without solvation due to the lack of analytical nuclear gradients for SS-PCM). At each geometry, all states are calculated under equilibrium solvation conditions (SS-PCM, solid levels), in the reaction field of the initial state ($SS^{initial}$-PCM, dashed levels), and under 1st-order non-equilibrium conditions (ptSS-PCM, dotted levels). For comparison, the experimental emission energies are drawn in black.

Combined, the CT emission energy $E_{em}^{1st,CT}$ is lower than $E_{em}^{1st,LE}$ by 0.62 and 0.79 eV for TDA-DFT and ΔUKS, respectively, confirming the assignment of the experimental emission to the CT state. Again, the non-equilibrium solvation effects for TDA-DFT and ΔUKS occur largely in parallel, yielding very similar emission energies for the CT state (E_{em}^{CT}=2.51 vs 2.48 eV). Both values agree excellently with the experiment (2.59 eV), especially when compared with the calculation in vacuum or the frequently employed TDA-DFT/LR-PCM (3.19 eV) level. These findings confirm that state-specific solvation, including appropriate non-equilibrium conditions for vertical transitions, cannot be neglected for either absorption or emission energies of competing low CT and LE states.

TDA-DFT — Following our detailed analysis of MCz-XT, we continue with the statistical evaluation of the entire STGABS27-EMS benchmark set, beginning with the results for TDA-DFT. Figure 3a) presents the statistical measures (mean absolute error MAE, mean deviation MD, and standard deviation SD) for TDA-DFT/ptSS-PCM with various density functionals.

A striking initial observation is the strong functional dependence of E_{em}, which ranges from the promising accuracy of OT-LRC-ωPBEh-D4 (green) to a substantial underestimation with PBE0-D4 (purple, MD ≈ −MAE = −0.73 eV). The crucial factor influencing performance is the fraction of non-local Fock exchange within the functional incorporated either globally (global hybrids) or range-dependent (range-separated hybrids). Increasing the global admixture, e.g., from 25% in PBE0-D4 to 37.5% in PBE38-D4 (blue), reduces the MAE by more than a factor of two, primarily due to a decrease in the negative MD accompanied by a minor reduction in SD. Among the optimally tuned RSHs, OT-LC-ωPBE-D4 (yellow, 0-100%) exhibits a similar error to PBE38-D4, while OT-LRC-ωPBEh-D4 (20-100%) and OT-ωB97M-V (red, 15-100%) are the most accurate. Interestingly, further analysis reveals a correlation between performance and Fock exchange fraction effective at the relevant electron-hole distance, as we already reported in a previous work.[16] For OT-LRC-ωPBEh, this fraction rises already around 0.7Å above the 37.5% of PBE38-D4 compared to 1Å for OT-LC-ωPBE (see Figure 2 in ref. 16). To understand this curious trend of decreasing errors with increasing Fock exchange, we re-

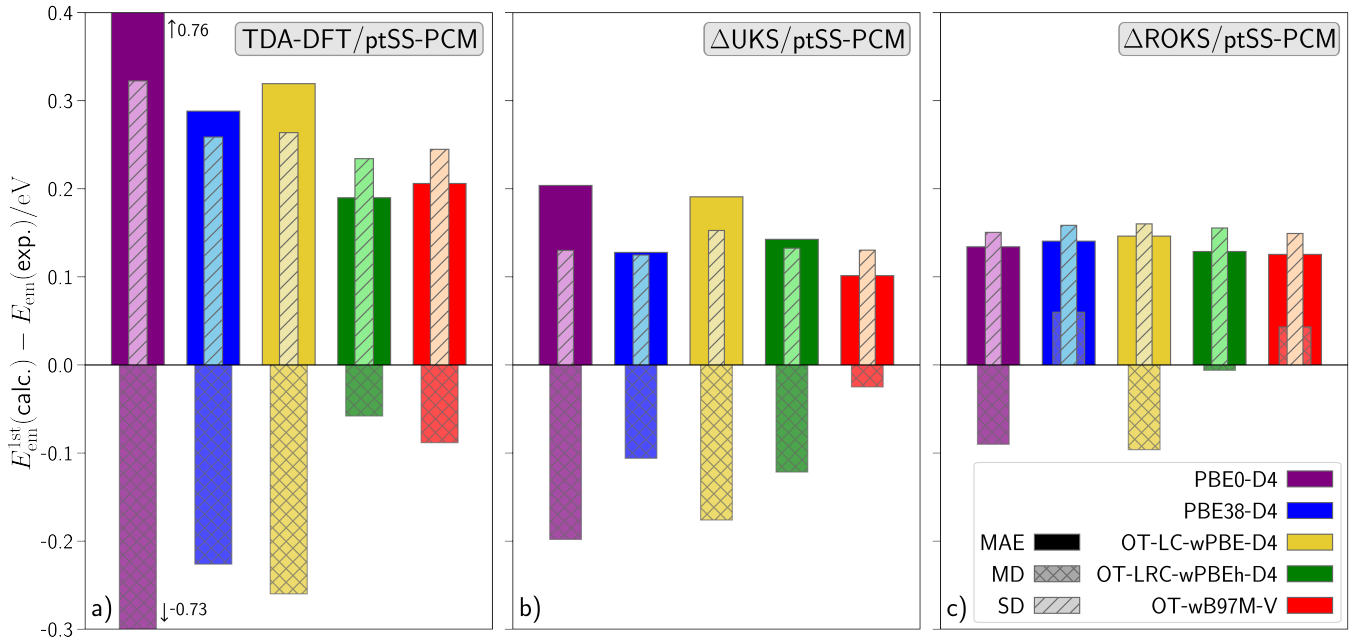

FIG. 3. Plots of the MAE (solid outer bar), MD (hatched middle bar), and SD (dashed inner bar) for the calculated $E_{\rm em}$ relative to the experimental reference. Values are shown for different functionals at the TDA-DFT/ptSS-PCM (a), UKS/ptSS-PCM (b), and ROKS/ptSS-PCM (c) level of theory. All calculations employ the S_1 optimized structures at the same level of theory (for TDA-DFT without solvation due to the lack of analytical nuclear gradients for SS-PCM).

visit our previous interpretation of the Fock exchange fraction as an effective dielectric screening between electron and hole ($\varepsilon \approx \frac{1}{a_{\rm x}}$, see ref. 16 for details). Since the SS-PCM already accounts for screening due to the dielectric continuum, we suspect that only a limited further screening (large $a_{\rm x}$) is required to mimic the effect of orbital relaxation. Notably, the opposite is true for predicting singlet-triplet gaps, where as little as 10% Fock exchange combined with an incomplete solvation model achieved the best performance with the help of a surprisingly stable error-compensation.[16] This highlights the need for comprehensive testing across different properties to avoid methods, which work primarily due to more or less stable fortuitous error cancellation. In general, the observed performance of TDA-DFT/ptSS-PCM is in line with previous studies, which reported MAEs between 0.2-0.3 eV for the emission from CT states of similar emitters.[22, 26, 106] Notably, these studies also reported benefits from both system-specifically optimally tuned RSHs and increased fractions of Fock exchange.

ΔDFT — After exploring the accuracy of TDA-DFT, we now turn to the ΔDFT-based methods. Figures 3 b) and c) illustrate the statistical analysis of the performance of ΔUKS/ptSS-PCM and ΔROKS/ptSS-PCM, respectively. From the start, it is clear that both are more consistent and provide much-improved emission energies than TDA-DFT. Across all tested functionals, the MAE and the magnitude of the MD are consistently below 0.2 eV, with the best-performing ΔUKS/OT-ωB97M-V achieving exceptional accuracy. Notably, this improved accuracy extends to the statistical error as measured by the SD, which is nearly halved compared to even the best TDA-DFT/SS-PCM method. This improvement of both systematic and statistical errors confirms that ΔDFT not only removes a systematic bias between experimental and calculated $E_{\rm em}$ values but leads to an overall more accurate description of the vertical emission process.

This improvement is clearly evident from the plot of the absolute emission energies ($E_{\rm em}$) against the experimental references depicted in Figure 4 (see Supporting information for plots including all tested methods): For OT-ωB97M-V, inspection shows that ΔDFT/ptSS-PCM (UKS in solid red, and ROKS in dashed orange lines) faithfully reproduces the relative trends in emission energies with only a few cases beyond the error range of 0.2 eV, whereas TDA-DFT/ptSS-PCM (purple, dash-dotted line) exhibits much larger deviations and more than a third of the cases at or clearly outside the 0.2 eV range. Selected examples include systems 14 and 15, where TDA-DFT underestimates the emission energies by over 0.5 eV, or 20, 21, and 22, which reverse their relative order, and all of which are accurately described by the ΔDFT-based methods. While seemingly acceptable in a benchmark considering mostly statistical performance, it should be noted that such severe deviations for several of the studied molecules can critically deteriorate the performance of screening and optimization tasks in material design.[107, 108] In this respect, having no outliers > 0.3 eV is more important than eliminating small statistical deviations of ≈ 0.1 eV

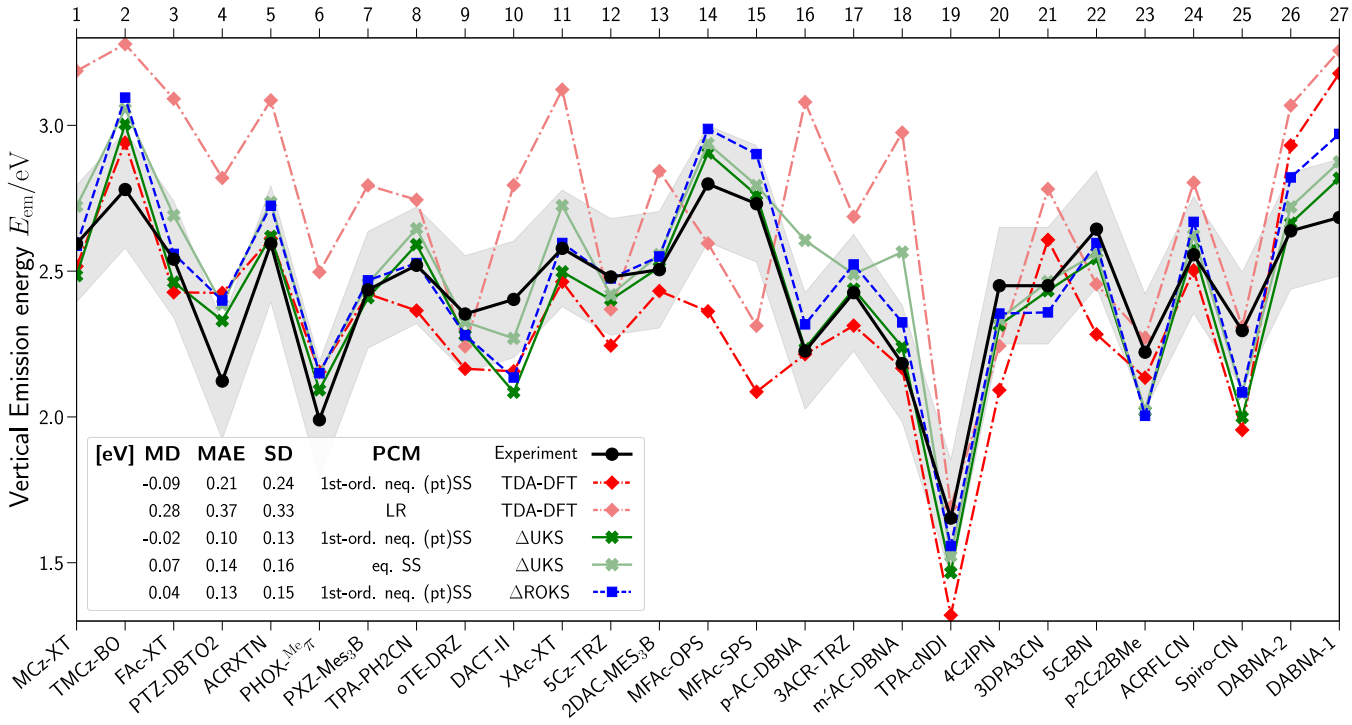

FIG. 4. Experimental (black) and calculated emission energies E_{em} for the emitters of the STGABS27 benchmark set. The calculated values are given for the OT-ωB97M-V functionals with TDA-DFT (red, dash-dotted), ΔUKS (green, solid), and ΔROKS (blue, dashed) at the consistently optimized S_1 geometry. Aside from 1st-order non-equilibrium state-specific solvation conditions (ptSS-PCM, full colors), TDA-DFT/LR-PCM (shaded red) and ΔUKS/SS-PCM under equilibrium conditions (shaded green) are plotted. ε and n^2 were chosen for the measurement-specific solvent (see Table I). An estimated uncertainty of ± 0.2 eV for the experimental reference is marked by a gray band. MD, MAE, and SD values for the set are tabulated.

Furthermore, we want to emphasize the remarkable robustness of the ΔDFT approaches regarding functional choice. In particular, the SD shows minimal variation across different functionals, regardless of the amount of admixed Fock exchange. Apart from a rather systematic shift towards smaller emission energies (negative MD), most functionals provide almost identical, highly accurate values for E_{em}. A remarkable example is the simple PBE38-D4 functional with ΔUKS/ptSS-PCM, which shows the lowest SD (0.13 eV) among all tested methods. This is particularly advantageous since it allows screening workflows without a sophisticated RSH or the computationally demanding system-specific optimal tuning procedure.

Having established the generally superior performance of time-independent ΔDFT/ptSS-PCM compared to the more common TD-DFT approach, we now turn to the choice of reference wavefunction for the open-shell singlet state. In other words: Is the formally correct ROKS approach so much better than UKS that the additional computational cost is justified? Comparing the emission energies for UKS (red) and ROKS (orange) with OT-ωB97M-V in Figure 4, both curves run largely parallel to each other, with ROKS predicting slightly higher E_{em} values (between 0.07-0.17 eV increase in MD). This systematic positive shift of ΔROKS (less negative MD) holds for all tested functionals. The explanation lies in the inherent difference between UKS and ROKS wavefunctions. ROKS incorporates two determinants for proper spin-adaptation, avoiding the unwanted admixture of the energetically close but lower triplet state known as spin-contamination. Interestingly, the statistical measures suggest a slight benefit from the spin-contamination in UKS. This even extends to the statistical error (SD) indicating that UKS is more accurate despite its formally incorrect handling of open-shell singlets, at least for the CT states studied herein. Hence, since the additional effort for ROKS offers no improvement in accuracy, the more widely available ΔUKS should be used for generally accurate emission energies of CT states.

Solvation models — After a detailed discussion of aspects of the electronic-structure method applied to the solute, let us now examine the influence of the solvent model for the dielectric environment. Figure 5 shows the statistical measures for TDA-DFT and ΔUKS with the OT-LRC-ωPBEh-D4 functional and different excited state solvation models. For TDA, there are several choices for the excited state solvation model: In addition to the physically complete LR-PCM or (pt)SS-PCM models, one may use the ground-state PCM or SS-PCM without first-order ptSS-corrections (SS$^{\mathrm{initial}}$). Here, we begin with TDA-DFT/SS-PCM under equilibrium con-

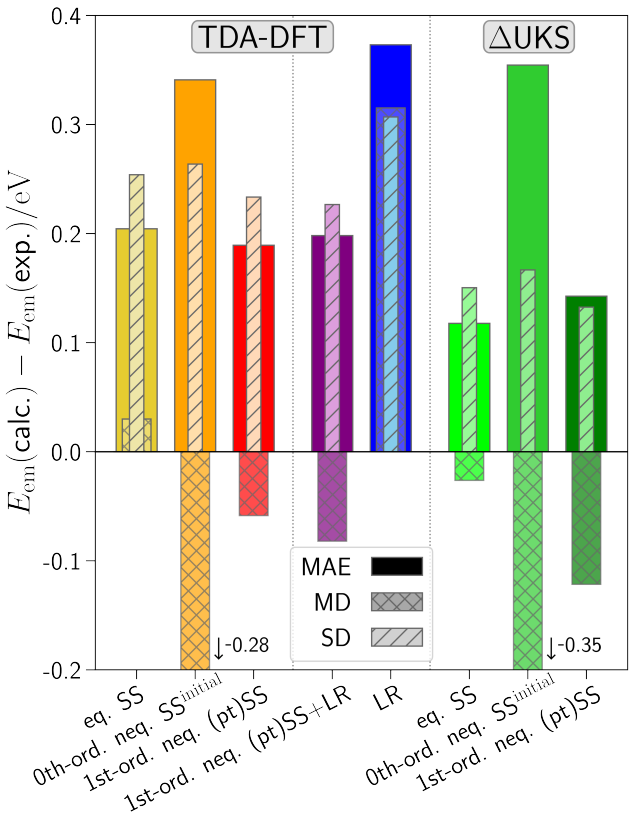

FIG. 5. Plots of the MAE (solid outer bar), MD (hatched middle bar), and SD (dashed inner bar) for the calculated E_{em} relative to the experimental reference. Values are shown for TDA-DFT and ΔUKS with different solvation models. All calculations use the OT-LRC-ωPBEh-D4 functional and S_1 optimized structures (for TDA-DFT without solvation).

ditions for ground and excited states ($E_{\mathrm{em}}^{\mathrm{eq}}$, yellow bar), which marginally overestimates the emission energies. However, non-equilibrium effects must be considered to account for the limited duration of the vertical emission process (see scheme in Figure 1). In the 0th-order $\mathrm{SS}^{\mathrm{initial}}$ approach ($E_{\mathrm{em}}^{\mathrm{0th}}$, orange bar), which neglects any solvent relaxation upon emission, E_{em} is systematically overestimated (negative MD), as we already saw in the exemplary case of MCz-XT (vide supra). Balanced emission energies require the relaxation of the fast electronic solvent DOFs at 1st-order via the ptSS-PCM correction ($E_{\mathrm{em}}^{\mathrm{1st}}$, red bar). Notably, the ptSS-PCM treatment also yields the lowest SD, which confirms the advantage of non-equilibrium solvation for vertical transitions. A similar trend emerges for the stepwise introduction of non-equilibrium solvation in the ΔUKS calculations, albeit at a substantially lower overall error (especially the SD). We can again compare the explicit emission energies predicted in the non-equilibrium (bright green) and equilibrium (shaded green) regimes displayed in Figure 4. Accounting for non-equilibrium solvation generally reduces the emission energies, though not uniformly by the same amount. The differences arise from the specific solvent used during measurement. Only polar solvents, where the total (ε) and infinite frequency (ε_∞) dielectric constants deviate substantially, such as DCM or PPF (Sys.: 1, 3, 11, 16, 18, 26, and 27), exhibit a significant non-equilibrium effect. Meanwhile, for non-polar solvents dominated by fast polarization, such as toluene, equilibrium and non-equilibrium conditions deviate only negligibly.

Knowing that sophisticated non-equilibrium solvation with the SS-PCM model for TDA-DFT works well, we also investigated the more widely available and often employed LR-PCM model. Benefits of LR-PCM compared to state-specific approaches include that the solvent response is treated for all states simultaneously and the availability of analytical gradients. However, a straightforward application of LR-PCM (blue bar) yields large errors stemming from a combined increase in the statistical error (larger SD) and a systematic overestimation of emission energies (positive MD). This is also apparent from the E_{em} values plotted in Figure 4 (dash-dotted shaded purple line). The substantial error arises from the near-zero contribution in the transition-density-based LR-PCM model, which is clearly a result of the vanishing transition density of polar CT states. Consequently, the simultaneous use of LR- and non-equilibrium SS-PCM, as suggested in ref. 68, also changes the results only slightly. Therefore, we conclude that any treatment of CT states with excitation-based models should include SS-PCM solvation since LR-PCM fails to recover the large dielectric stabilization of such states.

VI. CONCLUSIONS

We presented an extension of the STGABS27 benchmark set for singlet-triplet gaps to experimental emission energies E_{em}, termed STGABS27-EMS. This new data complements the existing singlet-triplet gaps ΔE_{ST} for 27 TADF emitters, allowing a more robust test for excited-state methods. The combined benchmark data probes polar CT states not only relative to each other[1, 16] but also relative to the non-polar ground state, which allowed us to refine our recommendations for treating charge transfer states in solution. In particular, STGABS27-EMS enabled us to explore the nuances of functional choice and excited state solvation for vertical transitions based on TDA-DFT and ΔDFT.

The primary result of this work is that ΔDFT/PCM-based approaches can predict emission energies of CT states of typical TADF emitters with higher accuracy and robustness than TDA-based approaches, as evident from the excellent mean absolute errors of 0.10 eV and standard deviation of 0.13 eV for the best-performing OT-ωB97M-V with ΔUKS/ptSS-PCM. Such deviations fall within our assumed maximum uncertainty for the reference E_{em} values, suggesting our initial estimate of 0.2 eV might be too conservative. Moreover, the ΔDFT accuracy shows at least a four times smaller sensitivity to

the functional choice than TDA-based approaches. Accordingly, the largest shift of the MD between the tested functionals is 0.67 eV for TDA-DFT, whereas the respective shift is just 0.17/0.16 eV for UKS/ROKS. TDA introduces systematic shifts in the emission energies and the accuracy depends more on the functional. This is evident from the SD, which varies between 0.23 and 0.32 eV for TDA, while it remains below 0.15/0.16 eV with UKS/ROKS. Hence, TDA calculations for CT require state-of-art range-separated hybrids in combination with optimal tuning and the sophisticated ptSS-PCM solvation model, whereas a ΔDFT calculation can employ any reasonable hybrid DFA, as evident from the good performance UKS/PBE38-D4. Clearly, the newly implemented non-equilibrium ptSS-PCM solvation for ΔDFT further improves the vertical emission energies, highlighting the general need for proper state-specific solvation.

In stark contrast, the most widely used excited state method TD(A)-DFT with SS-PCM solvation exhibits much larger deviations even with the best-performing OT-LRC-ωPBEh-D4 functional (MAE: 0.19 eV, SD: 0.23 eV). Unlike in our prior studies of singlet-triplet gaps, where a minimal admixture of $\approx$ 10% yields optimal error cancelation, emission energies require a large fraction of Fock exchange ($>$ 38%). Furthermore, we again confirmed the benefit of state-specific excited state solvation, as the commonly employed linear-response variant yields only a negligible stabilization over the vacuum. Although the best TDA-DFT/ptSS-PCM approach provides reasonable errors below 0.2 eV, it is not generally reliable for CT states in TADF emitters.

In conclusion, the combined benchmarking of ΔE_{ST} and E_{em} strongly suggests that ΔDFT/PCM methods provide a generally robust and accurate account of polar CT states in solution. This success can be attributed to (i) the explicit account for orbital relaxation, (ii) an inherently state-specific treatment of solvation, and (iii) the avoidance of the long-range CT failure of TD-DFT.

SUPPORTING INFORMATION

Detailed description of the computational workflow, methods, and used programs; complete plots of the emission energies for all used methods; investigation of basis set effects; definition of the used statistical measures

All optimized geometries of both singlet and triplet states as well as all used input and output files for the presented results.

CONFLICTS OF INTEREST

J.M.H. is part owner of Q-Chem and serves on its board of directors.

ACKNOWLEDGMENTS

T.F. acknowledges the Fonds der Chemischen Industrie (FCI) for funding under a Kekulé scholarship. This project has been funded with support from the RTG-2591 “TIDE-Template-designed Organic Electronics” by the DFG. J.M.H was supported by the U.S. National Science Foundation, grant no. CHE-1955282.

[1] Kunze, L.; Hansen, A.; Grimme, S.; Mewes, J. M. PCM-ROKS for the Description of Charge-Transfer States in Solution: Singlet-Triplet Gaps with Chemical Accuracy from Open-Shell Kohn-Sham Reaction-Field Calculations. *Journal of Physical Chemistry Letters* **2021**, *12*, 8470–8480.

[2] Zhang, Q.; Li, B.; Huang, S.; Nomura, H.; Tanaka, H.; Adachi, C. Efficient blue organic light-emitting diodes employing thermally activated delayed fluorescence. *Nature Photonics* **2014**, *8*, 326–332.

[3] Dias, F. B.; Penfold, T. J.; Monkman, A. P. Photophysics of thermally activated delayed fluorescence molecules. *Methods and Applications in Fluorescence* **2017**, *5*, 012001.

[4] Yang, Z.; Mao, Z.; Xie, Z.; Zhang, Y.; Liu, S.; Zhao, J.; Xu, J.; Chi, Z.; Aldred, M. P. Recent advances in organic thermally activated delayed fluorescence materials. *Chemical Society Reviews* **2017**, *46*, 915–1016.

[5] Wong, M. Y.; Zysman-Colman, E. Purely Organic Thermally Activated Delayed Fluorescence Materials for Organic Light-Emitting Diodes. *Advanced Materials* **2017**, *29*, 1605444.

[6] Samanta, P. K.; Kim, D.; Coropceanu, V.; Brédas, J.-L. Up-Conversion Intersystem Crossing Rates in Organic Emitters for Thermally Activated Delayed Fluorescence: Impact of the Nature of Singlet vs Triplet Excited States. *Journal of the American Chemical Society* **2017**, *139*, 4042–4051.

[7] Huang, T.; Jiang, W.; Duan, L. Recent progress in solution processable TADF materials for organic light-emitting diodes. *Journal of Materials Chemistry C* **2018**, *6*, 5577–5596.

[8] Mewes, J.-M. Modeling TADF in organic emitters requires a careful consideration of the environment and going beyond the Franck–Condon approximation. *Physical Chemistry Chemical Physics* **2018**, *20*, 12454–12469.

[9] Berberan-Santos, M. N.; Garcia, J. M. M. Unusually Strong Delayed Fluorescence of C70. *Journal of the American Chemical Society* **1996**, *118*, 9391–9394.

[10] Frank, I.; Hutter, J.; Marx, D.; Parrinello, M. Molecular dynamics in low-spin excited states. *The Journal of Chemical Physics* **1998**, *108*, 4060–4069.

[11] Kowalczyk, T.; Tsuchimochi, T.; Chen, P.-T.; Top, L.; Van Voorhis, T. Excitation energies and Stokes shifts from a restricted open-shell Kohn-Sham approach. *The Journal of Chemical Physics* **2013**, *138*, 164101.

[12] Gilbert, A. T. B.; Besley, N. A.; Gill, P. M. W. Self-Consistent Field Calculations of Excited States Using the Maximum Overlap Method (MOM). *The Journal of Physical Chemistry A* **2008**, *112*, 13164–13171.

[13] Barca, G. M. J.; Gilbert, A. T. B.; Gill, P. M. W. Simple Models for Difficult Electronic Excitations. *Journal of Chemical Theory and Computation* **2018**, *14*, 1501–1509.

[14] Miertuš, S.; Scrocco, E.; Tomasi, J. Electrostatic interaction of a solute with a continuum. A direct utilizaion of AB initio molecular potentials for the prevision of solvent effects. *Chemical Physics* **1981**, *55*, 117–129.

[15] Herbert, J. M. Dielectric continuum methods for quantum chemistry. *Wiley Interdisciplinary Reviews: Computational Molecular Science* **2021**, *11*, e1519.

[16] Froitzheim, T.; Grimme, S.; Mewes, J.-M. Either Accurate Singlet–Triplet Gaps or Excited-State Structures: Testing and Understanding the Performance of TD-DFT for TADF Emitters. *Journal of Chemical Theory and Computation* **2022**, *18*, 7702–7713.

[17] Runge, E.; Gross, E. K. U. Density-Functional Theory for Time-Dependent Systems. *Physical Review Letters* **1984**, *52*, 997–1000.

[18] Petersilka, M.; Gossmann, U. J.; Gross, E. K. U. Excitation Energies from Time-Dependent Density-Functional Theory. *Physical Review Letters* **1996**, *76*, 1212–1215.

[19] Hirata, S.; Head-Gordon, M. Time-dependent density functional theory within the Tamm–Dancoff approximation. *Chemical Physics Letters* **1999**, *314*, 291–299.

[20] Dreuw, A.; Head-Gordon, M. Failure of Time-Dependent Density Functional Theory for Long-Range Charge-Transfer Excited States: The Zincbacteriochlorin-Bacteriochlorin and Bacteriochlorophyll-Spheroidene Complexes. *Journal of the American Chemical Society* **2004**, *126*, 4007–4016.

[21] Dreuw, A.; Head-Gordon, M. Single-Reference ab Initio Methods for the Calculation of Excited States of Large Molecules. *Chemical Reviews* **2005**, *105*, 4009–4037.

[22] Shee, J.; Head-Gordon, M. Predicting Excitation Energies of Twisted Intramolecular Charge-Transfer States with the Time-Dependent Density Functional Theory: Comparison with Experimental Measurements in the Gas Phase and Solvents Ranging from Hexanes to Acetonitrile. *Journal of Chemical Theory and Computation* **2020**, *16*, 6244–6255.

[23] Jacquemin, D.; Wathelet, V.; Perpète, E. A.; Adamo, C. Extensive TD-DFT Benchmark: Singlet-Excited States of Organic Molecules. *Journal of Chemical Theory and Computation* **2009**, *5*, 2420–2435.

[24] Jacquemin, D.; Planchat, A.; Adamo, C.; Mennucci, B. TD-DFT Assessment of Functionals for Optical 0–0 Transitions in Solvated Dyes. *Journal of Chemical Theory and Computation* **2012**, *8*, 2359–2372.

[25] Jacquemin, D.; Moore, B. I.; Planchat, A.; Adamo, C.; Autschbach, J. Performance of an Optimally Tuned Range-Separated Hybrid Functional for 0–0 Electronic Excitation Energies. *Journal of Chemical Theory and Computation* **2014**, *10*, 1677–1685.

[26] Jacquemin, D.; Duchemin, I.; Blase, X. 0–0 Energies Using Hybrid Schemes: Benchmarks of TD-DFT, CIS(D), ADC(2), CC2, and BSE/GW formalisms for 80 Real-Life Compounds. *Journal of Chemical Theory and Computation* **2015**, *11*, 5340–5359.

[27] Jaunet-Lahary, T.; Laurent, A. D.; Laurence, C.; Medved', M.; Jacquemin, D. Exploring the Solvatochromism of Betaine 30 with Ab Initio Tools: From Accurate Gas-Phase Calculations to Implicit and Explicit Solvation Models. *Chemistry – A European Journal* **2017**, *23*, 4108–4119.

[28] Loos, P.-F.; Comin, M.; Blase, X.; Jacquemin, D. Reference Energies for Intramolecular Charge-Transfer Excitations. *Journal of Chemical Theory and Computation* **2021**, *17*, 3666–3686.

[29] Chai, J.-D.; Head-Gordon, M. Long-range corrected hybrid density functionals with damped atom–atom dispersion corrections. *Physical Chemistry Chemical Physics* **2008**, *10*, 6615–6620.

[30] Schirmer, J. Beyond the random-phase approximation: A new approximation scheme for the polarization propagator. *Physical Review A* **1982**, *26*, 2395–2416.

[31] Trofimov, A. B.; Schirmer, J. An efficient polarization propagator approach to valence electron excitation spectra. *Journal of Physics B: Atomic, Molecular and Optical Physics* **1995**, *28*, 2299.

[32] Christiansen, O.; Koch, H.; Jørgensen, P. The second-order approximate coupled cluster singles and doubles model CC2. *Chemical Physics Letters* **1995**, *243*, 409–418.

[33] Mester, D.; Kállay, M. Charge-Transfer Excitations within Density Functional Theory: How Accurate Are the Most Recommended Approaches? *Journal of Chemical Theory and Computation* **2022**, *18*, 1646–1662.

[34] Epifanovsky, E. et al. Software for the frontiers of quantum chemistry: An overview of developments in the Q-Chem 5 package. *The Journal of Chemical Physics* **2021**, *155*, 084801.

[35] Lee, J.; Aizawa, N.; Numata, M.; Adachi, C.; Yasuda, T. Versatile Molecular Functionalization for Inhibiting Concentration Quenching of Thermally Activated Delayed Fluorescence. *Advanced Materials* **2017**, *29*, 1604856.

[36] Kim, J. U.; Park, I. S.; Chan, C.-Y.; Tanaka, M.; Tsuchiya, Y.; Nakanotani, H.; Adachi, C. Nanosecond-time-scale delayed fluorescence molecule for deep-blue OLEDs with small efficiency rolloff. *Nature Communications* **2020**, *11*, 1765.

[37] Nobuyasu, R. S.; Ren, Z.; Griffiths, G. C.; Batsanov, A. S.; Data, P.; Yan, S.; Monkman, A. P.; Bryce, M. R.; Dias, F. B. Rational Design of TADF Polymers Using a Donor–Acceptor Monomer with Enhanced TADF Efficiency Induced by the Energy Alignment of Charge Transfer and Local Triplet Excited States. *Advanced Optical Materials* **2016**, *4*, 597–607.

[38] Inoue, M.; Serevilius, T.; Nakanotani, H.; Yoshida, K.; Matsushima, T.; Jurslnas, S.; Adachi, C. Effect of reverse intersystem crossing rate to suppress efficiency roll-off in organic light-emitting diodes with thermally activated delayed fluorescence emitters. *Chemical Physics Letters* **2016**, *644*, 62–67.

[39] Narsaria, A. K.; Rauch, F.; Krebs, J.; Endres, P.; Friedrich, A.; Krummenacher, I.; Braunschweig, H.; Finze, M.; Nitsch, J.; Bickelhaupt, F. M.; Marder, T. B. Computationally Guided Molecular Design to Minimize the LE/CT Gap in D-π-A Fluorinated Triarylboranes for Efficient TADF via D and π-Bridge Tuning. *Advanced Functional Materials* **2020**, *30*, 2002064.

[40] Suzuki, K.; Kubo, S.; Shizu, K.; Fukushima, T.; Wakamiya, A.; Murata, Y.; Adachi, C.; Kaji, H. Triarylboron-Based Fluorescent Organic Light-Emitting Diodes with External Quantum Efficiencies Exceeding 20 %. *Angewandte Chemie International Edition* **2015**, *54*, 15231–15235.

[41] Sommer, G. A.; Mataranga-Popa, L. N.; Czerwieniec, R.; Hofbeck, T.; Homeier, H. H. H.; Müller, T. J. J.; Yersin, H. Design of Conformationally Distorted Donor–Acceptor Dyads Showing Efficient Thermally Activated Delayed Fluorescence. *The Journal of Physical Chemistry Letters* **2018**, *9*, 3692–3697.

[42] Cai, X.; Qiao, Z.; Li, M.; Wu, X.; He, Y.; Jiang, X.; Cao, Y.; Su, S.-J. Purely Organic Crystals Exhibit Bright Thermally Activated Delayed Fluorescence. *Angewandte Chemie* **2019**, *131*, 13656–13665.

[43] Kaji, H.; Suzuki, H.; Fukushima, T.; Shizu, K.; Suzuki, K.; Kubo, S.; Komino, T.; Oiwa, H.; Suzuki, F.; Wakamiya, A.; Murata, Y.; Adachi, C. Purely organic electroluminescent material realizing 100% conversion from electricity to light. *Nature Communications* **2015**, *6*, 8476.

[44] Cui, L.-S.; Gillett, A. J.; Zhang, S.-F.; Ye, H.; Liu, Y.; Chen, X.-K.; Lin, Z.-S.; Evans, E. W.; Myers, W. K.; Ronson, T. K.; Nakanotani, H.; Reineke, S.; Bredas, J.-L.; Adachi, C.; Friend, R. H. Fast spin-flip enables efficient and stable organic electroluminescence from charge-transfer states. *Nature Photonics* **2020**, *14*, 636–642.

[45] Lee, J.; Aizawa, N.; Yasuda, T. Molecular engineering of phosphacycle-based thermally activated delayed fluorescence materials for deep-blue OLEDs. *Journal of Materials Chemistry C* **2018**, *6*, 3578–3583.

[46] Meng, G.; Chen, X.; Wang, X.; Wang, N.; Peng, T.; Wang, S. TADF Emitters: Isomeric Bright Sky-Blue TADF Emitters Based on Bisacridine Decorated DBNA: Impact of Donor Locations on Luminescent and Electroluminescent Properties (Advanced Optical Materials 11/2019). *Advanced Optical Materials* **2019**, *7*, 1970043.

[47] Wada, Y.; Shizu, K.; Kubo, S.; Suzuki, K.; Tanaka, H.; Adachi, C.; Kaji, H. Highly efficient electroluminescence from a solution-processable thermally activated delayed fluorescence emitter. *Applied Physics Letters* **2015**, *107*, 183303.

[48] Higginbotham, H. F.; Pander, P.; Rybakiewicz, R.; Etherington, M. K.; Maniam, S.; Zagorska, M.; Pron, A.; Monkman, A. P.; Data, P. Triphenylamine disubstituted naphthalene diimide: elucidation of excited states involved in TADF and application in near-infrared organic light emitting diodes. *Journal of Materials Chemistry C* **2018**, *6*, 8219–8225.

[49] Noda, H.; Chen, X.-K.; Nakanotani, H.; Hosokai, T.; Miyajima, M.; Notsuka, N.; Kashima, Y.; Brédas, J.-L.; Adachi, C. Critical role of intermediate electronic states for spin-flip processes in charge-transfer-type organic molecules with multiple donors and acceptors. *Nature Materials* **2019**, *18*, 1084–1090.

[50] Taneda, M.; Shizu, K.; Tanaka, H.; Adachi, C. High efficiency thermally activated delayed fluorescence based on 1,3,5-tris(4-(diphenylamino)phenyl)-2,4,6-tricyanobenzene. *Chemical Communications* **2015**, *51*, 5028–5031.

[51] Noda, H.; Nakanotani, H.; Adachi, C. Highly Efficient Thermally Activated Delayed Fluorescence with Slow Reverse Intersystem Crossing. *Chemistry Letters* **2019**, *48*, 126–129.

[52] Méhes, G.; Nomura, H.; Zhang, Q.; Nakagawa, T.; Adachi, C. Enhanced Electroluminescence Efficiency in a Spiro-Acridine Derivative through Thermally Activated Delayed Fluorescence. *Angewandte Chemie International Edition* **2012**, *51*, 11311–11315.

[53] Nakagawa, T.; Ku, S.-Y.; Wong, K.-T.; Adachi, C. Electroluminescence based on thermally activated delayed fluorescence generated by a spirobifluorene

donor–acceptor structure. *Chemical Communications* **2012**, *48*, 9580–9582.
[54] Nakanotani, H.; Furukawa, T.; Hosokai, T.; Hatakeyama, T.; Adachi, C. Light Amplification in Molecules Exhibiting Thermally Activated Delayed Fluorescence. *Advanced Optical Materials* **2017**, *5*, 1700051.
[55] Hatakeyama, T.; Shiren, K.; Nakajima, K.; Nomura, S.; Nakatsuka, S.; Kinoshita, K.; Ni, J.; Ono, Y.; Ikuta, T. Ultrapure Blue Thermally Activated Delayed Fluorescence Molecules: Efficient HOMO–LUMO Separation by the Multiple Resonance Effect. *Advanced Materials* **2016**, *28*, 2777–2781.
[56] Winget, P.; Dolney, D.; Giesen, D.; Cramer, C.; Truhlar, D. *Minnesota solvent descriptor database*; 1999.
[57] Vecchi, P. A.; Padmaperuma, A. B.; Qiao, H.; Sapochak, L. S.; Burrows, P. E. A Dibenzofuran-Based Host Material for Blue Electrophosphorescence. *Organic Letters* **2006**, *8*, 4211–4214.
[58] Skuodis, E.; Bezvikonnyi, O.; Tomkeviciene, A.; Volyniuk, D.; Mimaite, V.; Lazauskas, A.; Bucinskas, A.; Keruckiene, R.; Sini, G.; Grazulevicius, J. V. Aggregation, thermal annealing, and hosting effects on performances of an acridan-based TADF emitter. *Organic Electronics* **2018**, *63*, 29–40.
[59] Shih, P.-I.; Chien, C.-H.; Chuang, C.-Y.; Shu, C.-F.; Yang, C.-H.; Chen, J.-H.; Chi, Y. Novel host material for highly efficient blue phosphorescent OLEDs. *Journal of Materials Chemistry* **2007**, *17*, 1692–1698.
[60] Lasorne, B.; Jornet-Somoza, J.; Meyer, H.-D.; Lauvergnat, D.; Robb, M. A.; Gatti, F. Vertical transition energies vs. absorption maxima: Illustration with the UV absorption spectrum of ethylene. *Spectrochimica Acta Part A: Molecular and Biomolecular Spectroscopy* **2014**, *119*, 52–58.
[61] Tian, X.; Sun, H.; Zhang, Q.; Adachi, C. Theoretical predication for transition energies of thermally activated delayed fluorescence molecules. *Chinese Chemical Letters* **2016**, *27*, 1445–1452.
[62] Adamo, C.; Jacquemin, D. The calculations of excited-state properties with Time-Dependent Density Functional Theory. *Chemical Society Reviews* **2013**, *42*, 845–856.
[63] Laurent, A. D.; Jacquemin, D. TD-DFT benchmarks: A review. *International Journal of Quantum Chemistry* **2013**, *113*, 2019–2039.
[64] Tomasi, J.; Mennucci, B.; Cancès, E. The IEF version of the PCM solvation method: an overview of a new method addressed to study molecular solutes at the QM ab initio level. *Journal of Molecular Structure: THEOCHEM* **1999**, *464*, 211–226.
[65] Improta, R.; Barone, V.; Scalmani, G.; Frisch, M. J. A state-specific polarizable continuum model time dependent density functional theory method for excited state calculations in solution. *The Journal of Chemical Physics* **2006**, *125*, 054103.
[66] Improta, R.; Scalmani, G.; Frisch, M. J.; Barone, V. Toward effective and reliable fluorescence energies in solution by a new state specific polarizable continuum model time dependent density functional theory approach. *The Journal of Chemical Physics* **2007**, *127*, 074504.
[67] Cramer, C. J.; Truhlar, D. G.; Guido, C. A.; Mennucci, B.; Scalmani, G.; Frisch, M. J. Practical computation of electronic excitation in solution: Vertical excitation model. *Chemical Science* **2011**, *2*, 2143–2161.
[68] Mewes, J. M.; You, Z. Q.; Wormit, M.; Kriesche, T.; Herbert, J. M.; Dreuw, A. Experimental benchmark data and systematic evaluation of two a posteriori, polarizable-continuum corrections for vertical excitation energies in solution. *Journal of Physical Chemistry A* **2015**, *119*, 5446–5464.
[69] Mewes, J. M.; Herbert, J. M.; Dreuw, A. On the accuracy of the general, state-specific polarizable-continuum model for the description of correlated ground- and excited states in solution. *Physical Chemistry Chemical Physics* **2017**, *19*, 1644–1654.
[70] Guido, C. A.; Caprasecca, S. On the description of the environment polarization response to electronic transitions. *International Journal of Quantum Chemistry* **2019**, *119*, e25711.
[71] McRae, E. G. Theory of Solvent Effects on Molecular Electronic Spectra. Frequency Shifts. *The Journal of Physical Chemistry* **1957**, *61*, 562–572.
[72] Lippert, E. Lippert. *Z. Elektrochem.* **1957**, *61*, 952.
[73] Brady, J. E.; Carr, P. W. An analysis of dielectric models of solvatochromism. *The Journal of Physical Chemistry* **1985**, *89*, 5759–5766.
[74] Klamt, A. Calculation of UV/Vis Spectra in Solution. *The Journal of Physical Chemistry* **1996**, *100*, 3349–3353.
[75] You, Z. Q.; Mewes, J. M.; Dreuw, A.; Herbert, J. M. Comparison of the Marcus and Pekar partitions in the context of non-equilibrium, polarizable-continuum solvation models. *The Journal of Chemical Physics* **2015**, *143*, 204104.
[76] Caricato, M.; Mennucci, B.; Tomasi, J.; Ingrosso, F.; Cammi, R.; Corni, S.; Scalmani, G. Formation and relaxation of excited states in solution: A new time dependent polarizable continuum model based on time dependent density functional theory. *The Journal of Chemical Physics* **2006**, *124*, 124520.
[77] Yomosa, S. Theory of the Excited State of Molecular Complex in Solution. *Journal of the Physical Society of Japan* **1974**, *36*, 1655–1660.
[78] Bonaccorsi, R.; Cimiraglia, R.; Tomasi, J. Ab initio evaluation of absorption and emission transitions for molecular solutes, including separate consideration of orientational and inductive solvent effects. *Journal of Computational Chemistry* **1983**, *4*, 567–577.
[79] Cammi, R.; Corni, S.; Mennucci, B.; Tomasi, J. Electronic excitation energies of molecules in solution: State specific and linear response methods for nonequilibrium continuum solvation models. *The Journal of Chemical Physics* **2005**, *122*, 104513.
[80] Fukuda, R.; Ehara, M.; Nakatsuji, H.; Cammi, R. Nonequilibrium solvation for vertical photoemission and photoabsorption processes using the symmetry-adapted cluster–configuration interaction method in the polarizable continuum model. *The Journal of Chemical Physics* **2011**, *134*, 104109.
[81] Lunkenheimer, B.; Köhn, A. Solvent Effects on Electronically Excited States Using the Conductor-Like Screening Model and the Second-Order Correlated Method ADC(2). *Journal of Chemical Theory and Computation* **2013**, *9*, 977–994.
[82] Guido, C. A.; Jacquemin, D.; Adamo, C.; Mennucci, B. Electronic Excitations in Solution: The Interplay between State Specific Approaches and a Time-Dependent

Density Functional Theory Description. *Journal of Chemical Theory and Computation* **2015**, *11*, 5782–5790.

[83] Alam, B.; Jiang, H.; Zimmerman, P. M.; Herbert, J. M. State-specific solvation for restricted active space spin–flip (RAS-SF) wave functions based on the polarizable continuum formalism. *The Journal of Chemical Physics* **2022**, *156*, 194110.

[84] David Sherrill, C.; Schaefer, H. F. In *Advances in Quantum Chemistry*; Löwdin, P.-O., Sabin, J. R., Zerner, M. C., Brändas, E., Eds.; Academic Press, 1999; Vol. 34; pp 143–269.

[85] Emrich, K. An extension of the coupled cluster formalism to excited states (I). *Nuclear Physics A* **1981**, *351*, 379–396.

[86] Sekino, H.; Bartlett, R. J. A linear response, coupled-cluster theory for excitation energy. *International Journal of Quantum Chemistry* **1984**, *26*, 255–265.

[87] Cammi, R.; Mennucci, B. Linear response theory for the polarizable continuum model. *The Journal of Chemical Physics* **1999**, *110*, 9877.

[88] Corni, S.; Cammi, R.; Mennucci, B.; Tomasi, J. Electronic excitation energies of molecules in solution within continuum solvation models: Investigating the discrepancy between state-specific and linear-response methods. *The Journal of Chemical Physics* **2005**, *123*, 134512.

[89] Guido, C. A.; Mennucci, B.; Scalmani, G.; Jacquemin, D. Excited State Dipole Moments in Solution: Comparison between State-Specific and Linear-Response TD-DFT Values. *Journal of Chemical Theory and Computation* **2018**, *14*, 1544–1553.

[90] Budzák, S.; Scalmani, G.; Jacquemin, D. Accurate Excited-State Geometries: A CASPT2 and Coupled-Cluster Reference Database for Small Molecules. *Journal of Chemical Theory and Computation* **2017**, *13*, 6237–6252.

[91] Marcus, R. A. Electrostatic Free Energy and Other Properties of States Having Nonequilibrium Polarization. I. *The Journal of Chemical Physics* **1956**, *24*, 979.

[92] Marcus, R. A. On the Theory of Oxidation-Reduction Reactions Involving Electron Transfer. I. *The Journal of Chemical Physics* **1956**, *24*, 966.

[93] Stein, T.; Kronik, L.; Baer, R. Reliable Prediction of Charge Transfer Excitations in Molecular Complexes Using Time-Dependent Density Functional Theory. *Journal of the American Chemical Society* **2009**, *131*, 2818–2820.

[94] Baer, R.; Livshits, E.; Salzner, U. Tuned Range-Separated Hybrids in Density Functional Theory. *Annual Review of Physical Chemistry* **2010**, *61*, 85–109.

[95] Perdew, J. P.; Burke, K.; Ernzerhof, M. Generalized Gradient Approximation Made Simple. *Phys. Rev. Lett.* **1996**, *77*, 3865.

[96] Adamo, C.; Barone, V. Toward reliable density functional methods without adjustable parameters: The PBE0 model. *The Journal of Chemical Physics* **1999**, *110*, 6158.

[97] Goerigk, L.; Grimme, S. A thorough benchmark of density functional methods for general main group thermochemistry, kinetics, and noncovalent interactions. *Physical Chemistry Chemical Physics* **2011**, *13*, 6670–6688.

[98] Rohrdanz, M. A.; Herbert, J. M. Simultaneous benchmarking of ground- and excited-state properties with long-range-corrected density functional theory. *The Journal of Chemical Physics* **2008**, *129*, 034107.

[99] Rohrdanz, M. A.; Martins, K. M.; Herbert, J. M. A long-range-corrected density functional that performs well for both ground-state properties and time-dependent density functional theory excitation energies, including charge-transfer excited states. *The Journal of Chemical Physics* **2009**, *130*, 054112.

[100] Mardirossian, N.; Head-Gordon, M. ωB97M-V: A combinatorially optimized, range-separated hybrid, meta-GGA density functional with VV10 nonlocal correlation. *The Journal of Chemical Physics* **2016**, *144*, 214110.

[101] Caldeweyher, E.; Bannwarth, C.; Grimme, S. Extension of the D3 dispersion coefficient model. *The Journal of Chemical Physics* **2017**, *147*, 034112.

[102] Caldeweyher, E.; Ehlert, S.; Hansen, A.; Neugebauer, H.; Spicher, S.; Bannwarth, C.; Grimme, S. A generally applicable atomic-charge dependent London dispersion correction. *The Journal of Chemical Physics* **2019**, *150*, 154122.

[103] Friede, M.; Ehlert, S.; Grimme, S.; Mewes, J.-M. Do Optimally Tuned Range-Separated Hybrid Functionals Require a Reparametrization of the Dispersion Correction? It Depends. *Journal of Chemical Theory and Computation* **2023**, *19*, 8097–8107.

[104] Weigend, F.; Ahlrichs, R. Balanced basis sets of split valence, triple zeta valence and quadruple zeta valence quality for H to Rn: Design and assessment of accuracy. *Physical Chemistry Chemical Physics* **2005**, *7*, 3297–3305.

[105] Weigend, F. Accurate Coulomb-fitting basis sets for H to Rn. *Physical Chemistry Chemical Physics* **2006**, *8*, 1057–1065.

[106] Sun, H.; Zhong, C.; Brédas, J. L. Reliable Prediction with Tuned Range-Separated Functionals of the Singlet-Triplet Gap in Organic Emitters for Thermally Activated Delayed Fluorescence. *Journal of Chemical Theory and Computation* **2015**, *11*, 3851–3858.

[107] Jorner, K.; Pollice, R.; Lavigne, C.; Aspuru-Guzik, A. Ultrafast Computational Screening of Molecules with Inverted Singlet–Triplet Energy Gaps Using the Pariser–Parr–Pople Semiempirical Quantum Chemistry Method. *The Journal of Physical Chemistry A* **2024**, *128*, 2445–2456.

[108] Ricci, G.; San-Fabián, E.; Olivier, Y.; Sancho-García, J. C. Singlet-Triplet Excited-State Inversion in Heptazine and Related Molecules: Assessment of TD-DFT and ab initio Methods. *ChemPhysChem* **2021**, *22*, 553–560.